Tuning the copper(II) coordination properties of cyclam by subtle chemical modifications[i]

Nathalie Camus[a], Nathalie Le Bris[a], Selbi Nuryyeva[b,c], Matthieu Chessé[b], David Esteban-Gómez[d], Carlos Platas-Iglesias[d], Raphaël Tripier[a*] and Mourad Elhabiri[b†]

[a] Université de Bretagne Occidentale, UMR 6521 CNRS, SFR ScInBioS, UFR des Sciences et Techniques, 6 avenue Victor le Gorgeu, C.S. 93837, 29238 Brest Cedex 3, France

[b] Laboratoire de Chimie Bioorganique et Médicinale, UMR 7509 CNRS-Université de Strasbourg, ECPM, 25 Rue Becquerel, 67087 Strasbourg Cedex, France

[c] New York University Abu Dhabi (NYUAD), PO Box 129188, Abu Dhabi, United Arab Emirates

[d] Universidade da Coruña, Centro de Investigacións Científicas Avanzadas (CICA) and Departamento de Química, Facultade de Ciencias, 15071, A Coruña, Galicia, Spain

Dalton Transactions, volume 46, issue 34, pages 11479–11490, 14 September 2017
Received 01 March 2017, accepted 27 July 2017, first published 27 July 2017

How to cite:

Tuning the copper(II) coordination properties of cyclam by subtle chemical modifications. N. Camus, N. Le Bris, S. Nuryyeva, M. Chessé, D. Esteban-Gómez, C. Platas-Iglesias, R. Tripier and M. Elhabiri, *Dalt. Trans.*, 2017, **46**, 11479–11490. DOI: 10.1039/C7DT00750G.

Abstract

The acid–base and copper(II) coordination properties of three previously described cyclam derivatives are reported. Potentiometry, mass spectrometry, UV-vis absorption spectroscopy, electrochemistry and theoretical calculations were combined to investigate the protonation and binding properties of Bn-cyclam-EtOH (**L1**), oxo-cyclam-EtOH (**L2**) and oxo-Bn-cyclam-EtOH (**L3**). These three cyclams are *C*-functionalized by a hydroxyethyl pendant arm and display either one *N*-benzyl group and/or an amide replacing one macrocyclic secondary amine. The *N*-benzylic substitution has a significant effect of lowering the basicity of the corresponding protonation sites, while the presence of the amide function lowers the first protonation constants of the ligands. Regardless of the system considered, ESI mass spectrometry showed that only monocupric chelates are formed. Compared to the literature data, the stability constants measured by potentiometry (pCu **L1** = 14.67; pCu **L2** = 16.95; pCu **L3** = 15.28) showed that: (i) the *C*-appended group has a negligible influence on Cu^{2+} complexation, (ii) *N*-benzylation decreases the cupric complex stability, and (iii) the "oxo" function significantly increases the stability of the Cu^{2+} complex. Furthermore, UV-vis absorption *versus* pH measurements are in excellent agreement with the potentiometric titrations and show an equal involvement of the four nitrogen atoms in **L1** and the strong binding properties of **L2** and **L3** related to the deprotonation of the carboxamide. The electrochemistry parameters determined by cyclic voltammetry showed the predominance of the $[Cu\mathbf{L1}]^{2+}$, $[Cu\mathbf{L2}\text{-}H]^{+}$and $[Cu\mathbf{L3}\text{-}H]^{+}$ species but also the irreversibility of the three Cu^{2+}/Cu^{+} systems. Finally, density functional theory (DFT) and multiconfigurational CASSCF/NEVPT2 calculations confirmed that the protonation of the cupric complexes occurs at the oxygen atom of the amide group of the "oxo" ligands, which is in agreement with the experimental data.

* raphael.tripier@univ-brest.fr
† elhabiri@unistra.fr

Keywords: coordination compounds; DFT calculations; copper complexes; cyclam derivatives

Introduction

The extraordinary binding properties towards transition metal ions of azacycloalkane-based ligands and especially tetraazacycloalkanes, such as cyclam (1,4,8,11-tetraazacyclotetradecane), are now well recognized.[1] The high affinity of this aza backbone for copper(II), described by the HSAB principle,[2] is increasingly being used in numerous applications including the detection of cations and anions,[3] catalysis[4] and medicine.[5] For such uses, the azamacrocycle scaffold is generally modified or functionalized to fine-tune properties such as complexation and dissociation kinetics, thermodynamic stability, and the relative stability of the Cu^{2+} and Cu^{+} oxidation states, among others. Hence, the effect of *N*-functionalization has been intensively studied and evaluated for a large variety of applications.[6] However, the replacement of one or more amine groups of cyclam by an amide group has not been well investigated. This kind of chemical modification gives the so-called "oxo-" or "polyoxo-cyclam" ligands, which show features of both oligopeptides and saturated cyclic amines. They possess unusual acid–base properties due to the easy deprotonation of the amide proton(s). Protonation of these oxo-Cu^{2+} complexes may occur on the amide group either at the negatively charged nitrogen atom, with the metal–nitrogen bond being converted to a metal–oxygen bond,[7–10] or at the carbonyl oxygen without breaking the metal–nitrogen bond.[11] By taking advantage of the interesting properties of copper(II) complexes, the amide proton(s) on polyoxo-cyclam ligands can be replaced making them especially attractive as functional catalysts, in biological models of metalloproteins, systems for oxygen uptake and radiopharmaceuticals.

The *C*-functionalization of the macrocyclic skeleton is another interesting subtle modification that confers the macrocycle with an additional functionality for further derivatisation without alteration to its coordination properties. *C*-functionalization is usually accomplished at the β-*N* position of the cyclam backbone, so the additional arm is not expected to be involved in the coordination to the metal ion while allowing the metal complex to be anchored on a biomolecule, solid support, organic moiety, *etc*. However, there are only a few reports on physico-chemical approaches that investigate the real effect of the latter modification on the coordination properties, particularly when the appended group presents a heteroatom able to interact either with the macrocycle and/or the coordinated metal ion.[12]

We recently described the synthesis of cyclams *C*-functionalized on one carbon atom in the β-*N* position of the macrocycle, and also reported their assessment as ^{64}Cu chelators in new radiopharmaceuticals.[13] Among the various *C*-functionalized cyclams that have been synthesized, those bearing a hydroxyethyl function have been thoroughly investigated. Interestingly, the so-called cyclam-EtOH (Fig. 1) displayed acid–base and copper(II) coordination properties that are similar to the parent cyclam ligand. On the other hand, the synthetic routes that have been developed to obtain *C*-functionalized cyclams led to various key intermediates displaying a cyclic amide function that replaced an amine one and/or a regio-specific insertion of an *N*-benzyl function (oxo-cyclam-EtOH and oxo-Bn-cyclam-EtOH, Fig. 1). These synthetic intermediates thus deserve thorough physico-chemical investigations to analyse their properties for which, to the best of our knowledge, no information is available in the literature.

We aim to address several questions in this work. First, the effects of substitution of an amine by an amide group on the acid–base and Cu^{2+} complexation properties of the cyclam-EtOH macrocycle are investigated. The *N*-benzylation on the same macrocyclic scaffold is studied next. Ultimately, the consequences of these combined structural modifications (C-propylation, presence of an amide function and *N*-benzylation) on the cyclam backbone are evaluated. To further unravel the physico-chemical alterations of cyclams induced by these chemical functionalizations, we therefore investigated the acid–base and copper(II) complexation properties of Bn-cyclam-EtOH (**L1**), oxo-cyclam-EtOH (**L2**) and oxo-Bn-cyclam-EtOH (**L3**) (Fig. 1) using

potentiometric titrations, electrospray mass spectrometry, UV-vis absorption spectrophotometry, electrochemistry and theoretical calculations. Their properties will be discussed with respect to the simple cyclam, cyclam-EtOH, cyclam-*N*-PrOH and other oxo-cyclam derivatives.

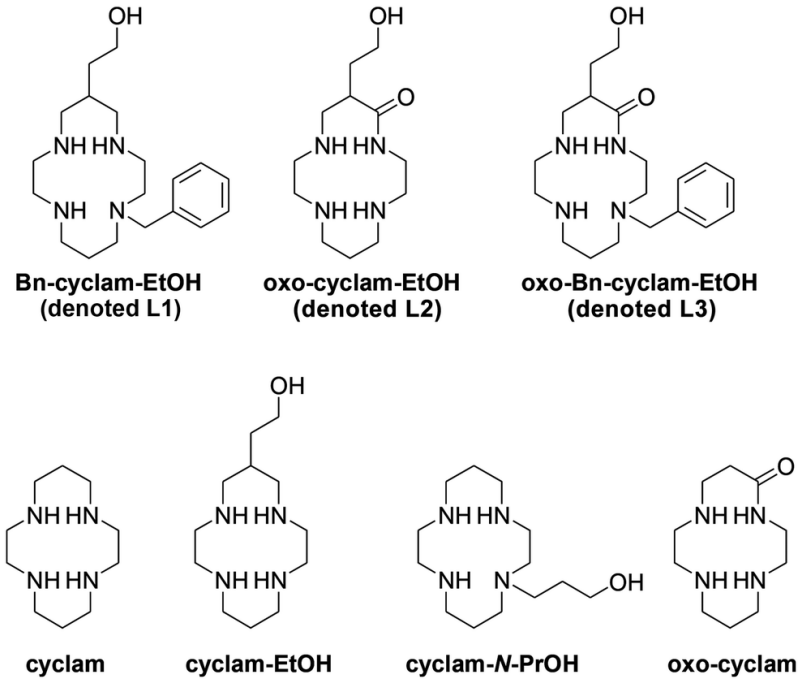

Fig. 1. Ligands studied and cited in this work.

Results and discussion

Ligand synthesis

The three ligands investigated herein were synthesized by following previously reported procedures involving bisaminal chemistry.[13a,c] This methodology is based on an organic template effect obtained by the condensation of a linear tetraamine with a dicarbonyl derivative (glyoxal or butanedione). This is followed by the cyclization of the resulting bisaminal with an α,β-unsaturated lactone (α-methylene-γ-butyrolactone), affording the double advantage (following various workups) of simultaneous amidation and selective mono-*N*-benzylation of the macrocycle.

Protonation properties

The acid–base properties of ligands **L1–L3** (Fig. 1) have been investigated by means of potentiometric (**L1–L3**) and ^{1}H NMR*versus* pH titration (**L1** and **L3**) measurements. The experimental titration curves are available in the ESI (Fig. S1–S3, S23 and S24[i]), whereas the protonation constants are gathered in Table 1. For the cyclam-based system **L1**, four protonation constants can be anticipated from the four ionizable amino sites. For the oxo-cyclams **L2** and **L3**, only three protonation constants were characterized. For **L1**, only the two highest protonation constants were accurately determined, similar to other related cyclam derivatives (Table S2, ESI[i]). A good agreement was obtained between the values determined in H_2O by potentiometry and those evaluated by ^{1}H NMR in D_2O, which were corrected for isotope effects.[14] The other protonation constants were estimated to be lower than 2 (log K_{013} = 2.43[15]/2.27[22] and log K_{014} = 1.97[15]/1.43[22] for cyclam),

mainly due to the electrostatic repulsions between the positive charges resulting from the successive protonations of the secondary (or tertiary) amines. For the oxo-cyclams, the three pK_a values that were accurately calculated are in excellent agreement with the literature data available for closely related systems (Table S2, ESI[i]). For **L3**, the value of the first protonation constant determined by ^{1}H NMR (*i.e.* log K_{011} = 10.8 recalculated assuming an isotope correction step) is in reasonably good agreement with that determined in H_2O by potentiometry.

Table 1. Logarithms of the protonation constants (log K_{alh}) [a,b] for ligands **L1–L3** [c]

	L1	**L2**	**L3**
$L + H^+ \rightleftharpoons LH^+ (\log K_{011})$	11.77(4)[d]	10.31(2)[d]	10.38(2)[d]
	11.68(9)[e]		10.8(1)[e]
$LH^+ + H^+ \rightleftharpoons LH_2^{2+} (\log K_{012})$	9.00(6)[d]	6.84(3)[d]	4.80(4)[d]
	9.43(1)[e]		
$LH_2^{2+} + H^+ \rightleftharpoons LH_3^{3+} (\log K_{013})$	≪2	2.62(6)[d]	2.59(7)[d]
$LH_3^{3+} + H^+ \rightleftharpoons LH_4^{4+} (\log K_{014})$	≪2	—	—

[a] $K_{alh} = [Cu_aL_lH_h]/[Cu_aL_lH_{h-1}][H]$ with $a = 0$, **L** = **L1–L3**. [b] Values in parentheses are standard deviations (3σ) in the last significant digit. [c] I = 0.100(8) M (NaCl); T = 25.0(2); [**L**] ~ 10^{-3} M. [d] potentiometry. [e] ^{1}H NMR *versus* pH titration in D_2O, I = 0.1 NaCl, T = 298 K (pK_a^* – pK_a measured in D_2O – are depicted in Table 1).

For **L1**, the first acid–base constant K_{011} can be attributed to the protonation of a secondary amine of the cyclam unit. The logarithmic value of K_{011} for **L1** (log K_{011} = 11.77(4)) is indeed comparable to the measured one in closely related systems such as cyclam (log K_{011} = 11.29,[16] log K_{011} = 11.59[17]), cyclam-*N*-PrOH (log K_{011} = 11.0)[18] or cyclam-EtOH (log K_{011} = 11.16). This first protonation step is thus characteristic of a secondary amine (*e.g.* log K_{011} = 11.02 for diethylamine[19] in water) with no stabilization of the ammonium ion by internal hydrogen bonds.

The second protonation of **L1** (log K_{011} = 9.00(6)) could be attributed to the tertiary amine opposite to the first protonation site (*i.e.* for charge minimization reasons) and agrees well with the value determined for cyclam-*N*-PrOH (log K_{011} = 9.24). Interestingly, this protonation constant is much lower than the value measured for the closely related cyclam-EtOH (log K_{011} = 10.14).

The relative magnitude of the second protonation constant is usually considered as a measure of the difficulty to protonate close to a positively charged centre. This second protonation constant is indeed lower than the first one because of the electrostatic interaction between the two positive charges borne by the ammonium cations ($\Delta\log K_H$ = 2.77 for **L1**, $\Delta\log K_H$ ~ 1.76 for cyclam-*N*-PrOH and $\Delta\log K_H$ ~ 1 for cyclam and cyclam-EtOH). Besides, it is worth mentioning that the *N*-benzylic substitution has also a significant effect of lowering the basicity of the corresponding protonation site. This feature was observed, for instance, on simple models such as 5-benzyldipropylenetriamine for which a decrease of more than two orders of magnitude was observed after the benzylic *N*-alkylation of the central secondary amine (Table S2, ESI[i]).[20]

The presence of the amide function for the macrocyclic oxo-tetraamines (*e.g.***L2** and **L3**) lowers the first protonation constant K_{011} by more than one order of magnitude, which can be attributed to a secondary

amino function. The measured log K_{011}values (10.31(2) for **L2** and 10.38(2) for **L3**) are in excellent agreement with the data obtained for the related oxo-cyclams lacking hydroxyethyl pendant arms. This can be explained by structural and electronic effects. Resonance effects centred on the amide unit result in a residual positive charge on the C=O carbon that contributes to a lower K_{011} value as a result of an electrostatic effect. Following this effect, the amide unit (C sp^2) has also a propensity to impose coplanarity on the N_4 binding system. With respect to the cyclam analogues, oxo-cyclam ligands display K_{012} values that are three orders of magnitude lower. These correspond to a much stronger electrostatic repulsions between adjacent ammonium cations that are induced by the presence of the carbonyl unit. It is noteworthy that the hydroxyethyl side arm has no effect on the protonation properties of **L1–L3**ligands. This is in contrast to the cyclam substituted on one nitrogen atom by a 3-hydroxypropyl group, which induces a decrease in both the ligand basicity and the stability of the metal complexes due to intramolecular hydrogen bonds between the hydroxyl group and the macrocyclic amines. The shorter hydroxyethyl pendant arm is unlikely to behave in a similar fashion. As a consequence, ligand **L2** displays comparable protonation constants to the analogous oxo-cyclam[7] lacking a hydroxyethyl substituent (log K_{011} = 10.31(2) *versus* 10.22; log K_{012} = 6.84(3) *versus* 7.02; log K_{013} = 2.62(6) *versus* 3.20). As already discussed for **L1**, *N*-alkylation with a benzylic moiety for **L3** markedly alters the protonation properties of the oxo-cyclam scaffold. The second protonation constant is further decreased by more than two orders of magnitude with respect to **L2** (log K_{012} = 4.80(4) for **L3** *versus* 6.84(3) for **L2**). The third protonation constants of **L2** and **L3** are comparable to the values of oxo-cyclam derivatives reported in the literature (log $K_{013} \sim$ 2.9–3.4).[7,10]

Coordination properties with Cu^{2+}

Mass spectrometry investigation: deprotonation of the amide unit. Prior to the physico-chemical investigations of the cupric complexes with ligands **L1–L3**, an ESI-MS study was carried out to elucidate the stoichiometry and the nature of the complexes formed in solution. Fig. 2 displays the ESI-MS spectra of the cupric complexes characterized with **L1** and **L3** (Fig. S4–S6, ESI[i], depict the ESI-MS spectra of ligands **L1–L3** and the cupric complexes with **L2**). Table 2 summarizes the results calculated from the ESI-MS spectra. Regardless of which system was considered, positively monocharged species were observed. For the free ligands, ionization occurs mainly through protonation. It is noteworthy that fragmentation occurs only for **L1** even under mild conditions (low skimmer voltage) and corresponds either to the loss of the benzyl substituent or to dehydration of the hydroxyethyl pendant arm. For the oxo-containing ligands **L2** and **L3**, no such fragmentations could be observed. With respect to the metal complexes, only monocupric chelates were characterized. For the cupric complexes with **L1**, ionization takes place primarily through the addition of counter-anions such as chloride and perchlorate arising out of the ligand or the cupric salt, respectively. It is noteworthy that fragments resulting from the loss of a water molecule at the hydroxyethyl substituent are still observed for the cupric complexes with **L1**. This suggests the absence of interactions between this substituent and the cyclam core, as has been shown for the protonated species (*vide supra*). For **L2** and **L3**, ionization of the cupric complexes occurs mainly through deprotonation of the NH amide function. This was already suggested for the oxo-cyclam derivatives[7–10] but never evidenced by mass spectrometric methods. Similar to **L1**, the addition of perchlorate counter-anions (resulting from the copper salt used) is also prone to form positively monocharged cupric species. These two cupric species with **L2** (or **L3**) likely correspond to the species in equilibrium.

Potentiometric data. Following the ESI-MS studies, the stability constants of the Cu^{2+} complexes with **L1–L3** were then evaluated by means of potentiometric titrations. Fig. S7–S9 (see the ESI[i]) show the experimental potentiometric titrations and the corresponding statistical analyses of the cupric complexes, while Table 3 gathers the resulting stability constants that were determined. In all systems, only the anticipated monocupric chelates were evidenced by potentiometry, which is in agreement with the preliminary ESI-MS studies (*vide supra*). Moreover, the stability constant measured for the Cu^{2+} complex with **L1**compares well with those measured for the *N*-substituted cyclam-*N*-PrOH analogue (Table 3).

However, it was found that **L1**(pCu = 14.67) is stabilized with respect to cyclam-*N*-PrOH (pCu = 12.70) as a consequence of the absence of interaction with the hydroxyethyl pendant arm. Indeed, it has been demonstrated for cyclam-*N*-PrOH that intramolecular hydrogen bonding of the propanol chain with the cyclam scaffold preorganizes the ligand against complexation and thereby destabilises the cupric complexes.[18] To a certain extent, the cupric complexes with **L1** are destabilised with respect to cyclam-EtOH (pCu = 18.04) or cyclam (pCu = 20.04) as a consequence of *N*-alkylation that tends to decrease the overall basicity of the ligand (for **L1**: $\log K_{011} + \log K_{012} = 20.77$ and for cyclam-*N*-PrOH: $\log K_{011} + \log K_{012} = 20.24$ *versus* for cyclam-EtOH: $\log K_{011} + \log K_{012} = 21.3$ and for cyclam: $\log K_{011} + \log K_{012} = 21.89$[15]). Steric hindrance brought by the *N*-benzylation may also partially explain this destabilisation. The speciation diagram measured for the Cu^{2+} complex with **L1** (Fig. 3) shows that the monocupric chelate predominates in a broad pH range from 3 to 12, the complex dissociating at acidic pH values (pH < 3). In addition to the expected monocupric chelate $[Cu\mathbf{L2}]^{2+}$, the potentiometric titration data of the monooxo-tetraamine system **L2** undoubtedly showed the formation of the monodeprotonated complex $[Cu(\mathbf{L2}\text{-H})]^{+}$ with an associated acidic pK_a value of 3.87(6). The Cu^{2+}coordination properties of **L2** (pCu = 16.72) are comparable to those of the unsubstituted monooxo-cyclam (pCu = 17.62, Table 3) and demonstrate a negligible influence of the hydroxyethyl substitution. The measurement of the pCu values at pH 7.4 for **L2**(pCu = 16.95) also suggested a stabilization of the cupric complex with respect to **L1** (pCu = 14.67) and only a moderate destabilisation with respect to cyclam-EtOH (pCu = 18.04), thus indicating that on subtle modification of the cyclam to monooxo-cyclam scaffolds, the Cu^{2+} complexation properties are preserved while allowing the decrease of the global charge of the cupric complex. Upon deprotonation of the amide function of $[Cu\mathbf{L2}]^{2+}$, a possible resonance stabilisation of the resulting carboximidate anions likely imposes coplanarity on the **N4** donor set. This process is undoubtedly triggered by copper(II) complexation and deprotonation of the cupric complex. The Cu^{2+} speciation diagram of **L2** also shows that the Cu^{2+}monochelates predominate in a broad pH range (3 < pH < 12). Similar to **L1***versus* cyclam-EtOH, the decrease of basicity due to*N*-benzylation for **L3** ($\log K_{011} + \log K_{012} = 15.18$) – with respect to **L2** ($\log K_{011} + \log K_{012} = 17.15$) – is a plausible explanation of the destabilisation of the Cu^{2+} complexes with **L3** (pCu = 15.28). As a matter of fact, only the deprotonated cupric complex $[Cu(\mathbf{L3}\text{-H})]^{+}$ was accurately characterized ($\log K_{11-1} = 9.91(4)$). Again, comparison of the Cu^{2+} coordination properties of **L3** with**L1** or cyclam-*N*-PrOH (Table 3) demonstrates that the incorporation of an oxo function within the cyclam core has a tendency to increase the stability of the corresponding cupric complexes (Fig. S25–S27, ESI[i]).

Table 2. Intensity maxima of the ESI-MS pseudo-molecular ions of the metallic complexes formed with ligands **L1–L3**[a]

Ligand			Cupric complexes		
Species	*m/z* exp.	*m/z* calc.	Species	*m/z* exp.	*m/z* calc.
$[\mathbf{L1} + H - Bn]^{+}$	245.25	245.23	$[\mathbf{L1} + Cu + Cl - H_2O]^{+}$	414.25	414.17
$[\mathbf{L1} + H - H_2O]^{+}$	317.35	317.27	$[\mathbf{L1} + Cu + Cl]^{+}$	432.30	432.18
$[\mathbf{L1} + H]^{+}$	335.35	335.28	$[\mathbf{L1} + Cu + ClO_4]^{+}$	496.30	496.18
$[2\mathbf{L1} + 2H + Cl]^{+}$	705.70	705.53			
$[\mathbf{L2} + H]^{+}$	259.30	259.21	$[\mathbf{L2} + Cu - H]^{+}$	320.20	320.14
	420.20	420.09	$[\mathbf{L2} + Cu + ClO_4]^{+}$		
$[\mathbf{L3} + H]^{+}$	349.35	349.26	$[\mathbf{L3} + Cu - H]^{+}$	410.30	410.18
$[2\mathbf{L3} + H + Cl]^{+}$	733.60	733.48	$[\mathbf{L3} + Cu + ClO_4]^{+}$	510.25	510.14

[a] Solvent: H_2O. Positive mode; skimmer voltage ranged from 150 V to 200 V. $[\mathbf{L}]_0 \sim 5 \times 10^{-5}$ M. $[Cu^{2+}]_0/[\mathbf{L}]_0 \sim 1$. Bn = benzyl.

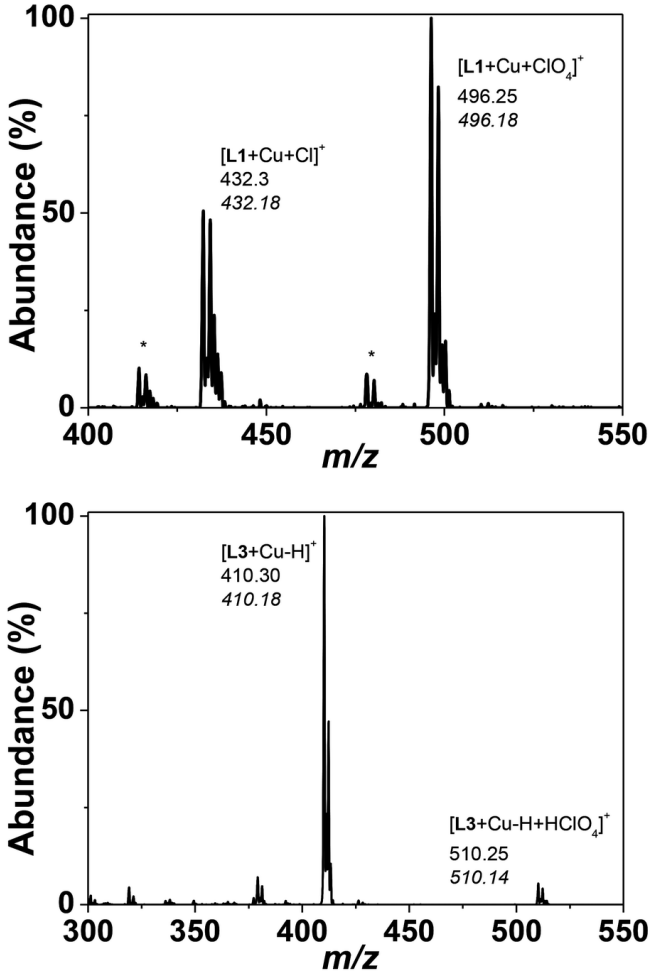

Fig. 2. ESI-MS spectra of the cupric complexes with **L1** (top) and **L3** (bottom). Solvent: H_2O; positive mode. (a) $[Cu^{2+}]_0 = [\mathbf{L1}]_0 = [\mathbf{L3}]_0 = 5 \times 10^{-5}$ M; (for **L1**), V_c = 100 V; (for **L3**) V_c = 150 V. The ESI-MS spectra were limited to the areas of interest. No peaks of interest were detected in the excluded *m*/*z* regions.

UV-vis absorption versus pH measurements. In addition to the potentiometric investigations described above, a UV-vis absorption spectrophotometric characterisation of the monocupric complexes as a function of pH has also been performed. The cupric complexes with **L1–L3** (*i.e.* prepared by mixing equimolar amounts of both the ligand and Cu^{2+} perchlorate) all displayed interesting spectroscopic signatures such as an intense N → Cu^{2+} charge transfer (LMCT)[26] absorption in the UV region and weaker Cu^{2+} d–d transitions in the visible spectral window (Table 4). For **L1**, which is lacking an oxo unit in the cyclam skeleton, no spectral variation was observed in agreement with the high stability of the **L1** cupric complex (Table 3) and the absence of (de)protonation reactions on a broad pH range (Fig. S10, see the ESI[i]). The spectral characteristics of the Cu^{2+} d–d transitions (λ_{max} = 528 nm) with ligand **L1** suggested a distorted square planar N4 geometry in agreement with equal involvement of the four nitrogen atoms to Cu^{2+} binding.[27] The cupric complexes with the oxo-containing cyclam ligands **L2** and**L3** stand in an interesting contrast since a large spectral variation can be observed under acidic pH (Fig. 4 and Fig. S11, see the ESI[i] for **L2** and Fig. S12, see the ESI[i] for **L3**), which is in agreement with the deprotonation of the carboxamide unit shown by ESI-MS or potentiometric results (*vide supra*).

Firm binding to the cupric centre and concomitant deprotonation of the carboxamide (*i.e.* leading to carboximidate anion) are characterized by a large hyperchromic shift of the N → Cu^{2+} charge transfer (LMCT) absorption. Under the deprotonated state, the LMCT bands arising from the [Cu**L**-H]$^+$ species with **L2** and **L3** are comparable to that of the cupric complex [Cu**L1**]$^{2+}$with the cyclam-based

ligand **L1** (Table 4) suggesting a similar N4 coordination arrangement. This was further evidenced by the maximum absorption of $[Cu\mathbf{L1}]^{2+}$ (λ_{max} = 528 nm) d–d transitions that is similar to those ($[Cu\mathbf{L}]^{2+}$ and $[Cu\mathbf{L}\text{-}H]^{+}$) with the oxo-cyclam ligands **L2** (λ_{max} = 534 nm and 519 nm) and **L3** (λ_{max} = 507 nm), thus indicating a comparable macrocyclic square planar N4 ligand field in any protonated state of the cupric complex. The fact that the shift of the d–d transitions between $[Cu\mathbf{L}\text{-}H]^{+}$and $[Cu\mathbf{L}]^{2+}$ for **L2** is relatively small indeed suggests that the same CuN4 chromophore is present in all of these species. Since the protonation does not displace a nitrogen atom from the coordination sphere of the cupric ion, it is therefore implied that the deprotonation must take place at the carbonyl oxygen following a prototropic tautomeric process. Involvement of the chloride anions in the Cu^{2+} coordination sphere is most likely negligible as shown by the relatively weak shift of the d–d transitions measured upon addition of an excess of NaCl to aqueous solutions (I = 0 M) of the cupric complexes with **L1–L3** (Fig. S13–S17, see the ESI[i]). Lastly, it is worth mentioning that the stability and deprotonation constants measured for the cupric complexes with **L2** and **L3** by UV-vis absorption *versus* pH titrations are in excellent agreement with those determined by potentiometric means (Table 3).

Table 3. Stepwise constants (logarithms of the stability and protonation constants ($\log K_{alh}^{a,b}$)) determined for the free ligands **L1–L3** and the corresponding cupric complexes[c] and compared to closely related systems (see Fig. 1 for the chemical structures)

	Equilibrium	**L1** Bn-cyclam-EtOH	Cyclam	Cyclam-EtOH	Cyclam-*N*-PrOH
$\log K_{110}$	$\mathbf{L} + Cu^{2+} \rightleftharpoons [Cu\,\mathbf{L}]^{2+}$	19.7(2)[c]	26.51[e]	23.6(1)[f]	17.2(1)[g]
			26.5(1)[h]		
			28.1[i]		
$\log K_{111}$	$[Cu\,\mathbf{L}]^{2+} + H^{+} \rightleftharpoons [Cu\,\mathbf{L}H]^{3+}$	—	—	2.9(1)[f]	—
$\log K_{11\text{-}1}$	$[Cu\,\mathbf{L}]^{2+} \rightleftharpoons [Cu(OH)\mathbf{L}]^{+} + H^{+}$	—	—	−10.8(2)[f]	−10.5[g]
	pCu[l] (pH 7.4)	14.67	20.04	18.04	12.70
Equilibrium	**L2** Oxo-cyclam-EtOH	**L3** Oxo-Bn-cyclam-EtOH	Oxo-cyclam		
$\log K_{110}$	$\mathbf{L} + Cu^{2+} \rightleftharpoons [Cu\,\mathbf{L}]^{2+}$	15.46(4)[c]	nd[m]	16.76(2)[j]	
		15.0(2)[d]	nd[m]	16.15[k]	
$\log K_{11\text{-}1}$	$[Cu\,\mathbf{L}]^{2+} \rightleftharpoons [Cu\,\mathbf{L}\text{-}\mathbf{H}]^{+} + H^{+}$	−3.87(6)[c]	$\log \beta_{11-1}$ = 9.91(4)[c]	−3.76(5)[j]	
		−3.8(4)[d]	$\log \beta_{11-1}$ = 9.67(6)[d]	−3.18[k]	
		16.95	15.28	17.62	

[a] $K_{alh} = [Cu_aL_lH_h]/[Cu_aL_lH_{h-1}][H]$ with a = 1, L = **L1–L3**. [b] Values in parentheses are standard deviations (3σ) in the last significant digit. [c] This work; H_2O; 0.1 M NaCl, 25 °C, potentiometry. [d] This work; H_2O; 0.1 M NaCl, 25 °C, UV-vis absorption *versus* pH. [e] H_2O, 0.1 M KNO_3, K_2H_2edta solution, 25 °C, ref. 21. [f] H_2O, 0.1 M KNO_3, K_2H_2edta solution, 25 °C, ref. 13*a*. [g] H_2O; 0.1 M NEt_4ClO_4, ref. 18. [h] H_2O; 0.5 M $NaNO_3$, ref. 22. [i] Ref. 23. [j] H_2O; 0.5 M KNO_3, 25 °C, ref. 7 and 10. [k] H_2O; 0.1 M KCl, 25 °C, ref. 7. [l] pCu = $[Cu^{2+}]_{free}$ for $[\mathbf{L}] = 10^{-5}$ M and $[Cu] = 10^{-6}$ M and pH 7.4, ref. 24 pCu measures the complexation efficiency of the ligands and takes into account the difference in basicity of the ligands and in the stoichiometries of the cupric complexes. $\log K_{Cu(OH)^+} = -6.29$ and $\log K_{Cu(OH)2} = -13.1$ ref. 25. [m] nd = not determined with good accuracy.

Electrochemical properties. The inertness of copper(II) complexes with respect to their dissociation upon reduction to labile Cu^{+} species is an important physico-chemical outcome for $^{64}Cu/^{67}Cu$ chelate candidates when considered for any potential use in nuclear medicine for imaging or therapeutic techniques (*e.g.* PET or RIT, respectively). Reduction of the cupric complexes by endogenous bioreducers can indeed afford unstable and labile Cu^{+} species that can undergo dissociation by solvolysis, acidolysis or ligand exchange. As a result, the metal can spread in the body and consequently lead to the loss of selectivity with respect to the target to be imaged, as well as undesirable health effects. To partly assess these properties, the electrochemical properties of the cupric complexes with **L1–L3** have been investigated by cyclic voltammetry (CV, Table 5).

CV voltamperograms were recorded in water at pH 7.4 (HEPES 0.05 M + 0.095 M $NaClO_4$) as an electrolyte support at 25 °C with a glassy carbon working electrode. Fig. S18–S20 (see the ESI[i]) display the CV graphs measured for millimolar solutions of Cu**L** (**L** = **L1**–**L3**).

Under these experimental conditions, the cupric complexes predominate under doubly positively charged species for **L1**($[Cu\mathbf{L1}]^{2+}$) and positively monocharged species for either **L2** or **L3** ($[Cu\mathbf{L2}\text{-}H]^{+}$ and $[Cu\mathbf{L3}\text{-}H]^{+}$, Fig. 3). For the sake of clarity, the CV of a millimolar solution of $Cu(ClO_4)_2$ has been recorded as well. For $[Cu\mathbf{L1}]^{2+}$ at pH 7.4, an irreversible reduction wave at E_{pc} = −0.88 V *versus* Ag/AgCl/(3 M KCl) can be observed without clear support of re-oxidation of the cuprous complex. Instead, an oxidation peak characteristic of Cu^0 to Cu^{2+} close to +0.2 V *versus* Ag/AgCl/(3 M KCl) is observed. This so-called anodic stripping or redissolution peak (caused by the redissolution of metallic copper) is a clear signature of Cu^0 formation due to the dismutation of dissociated Cu^+ ions. This suggests that the electrogenerated Cu^+ complex derived from ligand **L1** is unstable and dissociates during the timescale of the electrochemical experiment.[28] Moreover, no oxidation of the cupric complex to Cu^{3+} can be observed. For $[Cu\mathbf{L2}\text{-}H]^{+}$, the electrochemical measurements also indicated an irreversible cathodic signal at E_{pc} = −0.50 V *versus* Ag/AgCl/(3 M KCl) and an irreversible oxidation peak at E_{pa} = +0.34 V *versus* Ag/AgCl/(3 M KCl). Cathodic and anodic signals related to the redissolution and redox processes of metallic copper can be also detected. Similar to $[Cu\mathbf{L1}]^{2+}$, the $[Cu\mathbf{L2}\text{-}H]^{+}$ species displays a comparable CV profile with an irreversible reduction peak at −0.87 V *versus* Ag/AgCl/(3 M KCl). The reduction process observed for the Cu^{2+} complex with **L1** or **L3** (E_{pc} = −0.66 V/NHE) is well below the estimated potential threshold (−0.40 V/NHE) for typical bioreductants, which suggests that complex dissociation upon Cu^{2+} reduction in biological media is unlikely. However, the irreversibility of this electrochemical process, arising from the stereochemical constraints induced by the chelating unit for Cu^+ species, is a limitation that has to be taken into account for further development.

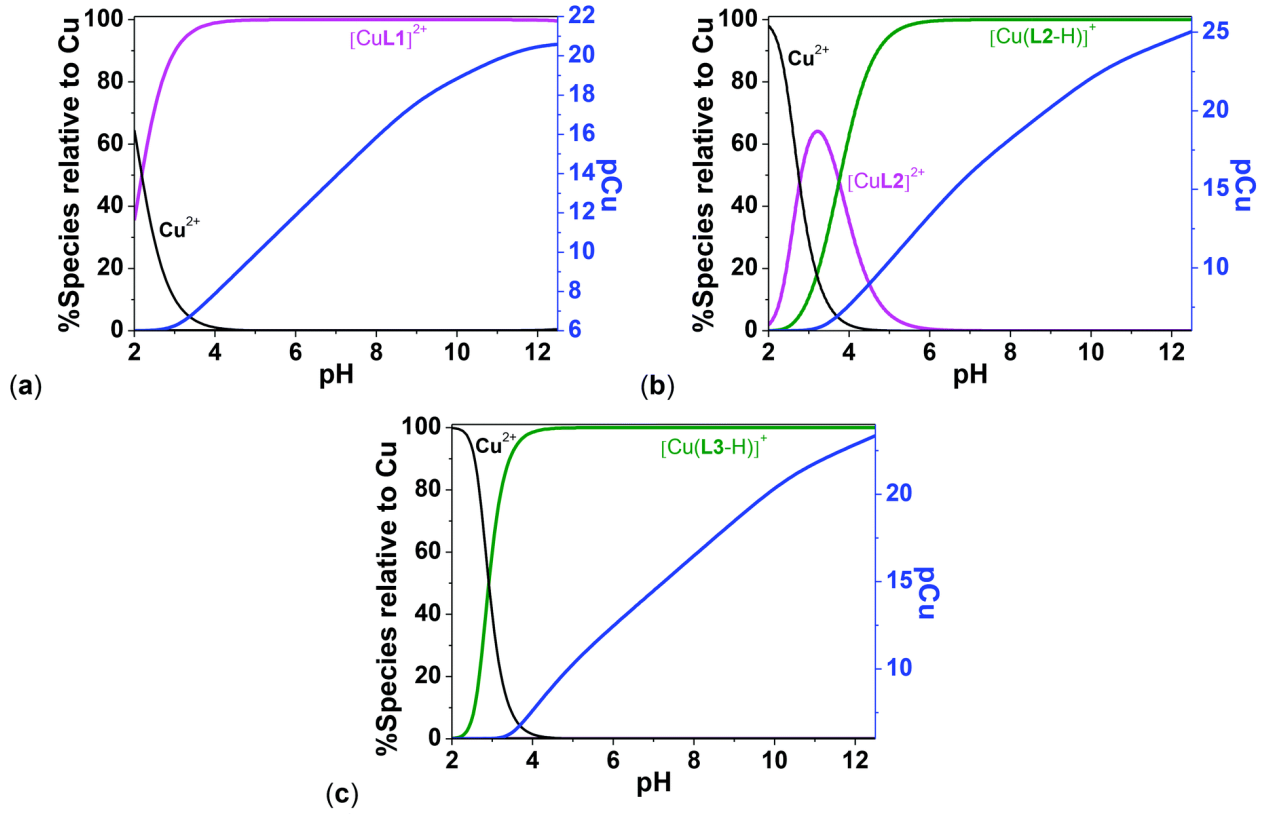

Fig. 3. Cu^{2+} speciation diagrams and pCu values of (a) **L1**, (b) **L2** and (c) **L3** as a function of pH. $[Cu^{2+}]_0 = [\mathbf{L}]_0 = 10^{-3}$ M. pCu = $[Cu^{2+}]_{free}$ for [**L**] = 10^{-5} M and [Cu] = 10^{-6} M. H_2O; 0.1 M NaCl, 25 °C.

Table 4. UV-vis absorption spectrophotometric parameters of the cupric complexes formed with ligands **L1–L3** [a]

	λ^{max} ($\varepsilon^{\lambda max}$)/nm ($M^{-1}$ cm^{-1})	
Species	N → Cu^{2+} LMCT	Cu^{2+} d–d
L1	251(340)/257(315)/264(240)	[b]
	sh ~ 320	
[Cu**L1**]$^{2+}$	269 (5500)	528(150)
L2	sh ~ 305	[b]
[Cu**L2**]$^{2+}$	257(4330)	534(70)
[Cu**L2**-H]$^{+}$	253(4900)	519(85)
L3	252(470)/258(485)/264(442)/311(360)	[b]
[Cu**L3**]$^{2+}$	nd	nd
[Cu**L3**-H]$^{+}$	263(5930)	507(130)

[a] From the statistical processing of the absorption *versus* pH titrations. Solvent: water; I = 0.100(8) M NaCl; T = 25.0(2) °C. [b] No Cu^{2+} d–d transitions. The errors on λ and ε are estimated to be ~±1 nm and 10%, respectively. nd = not determined with good accuracy.

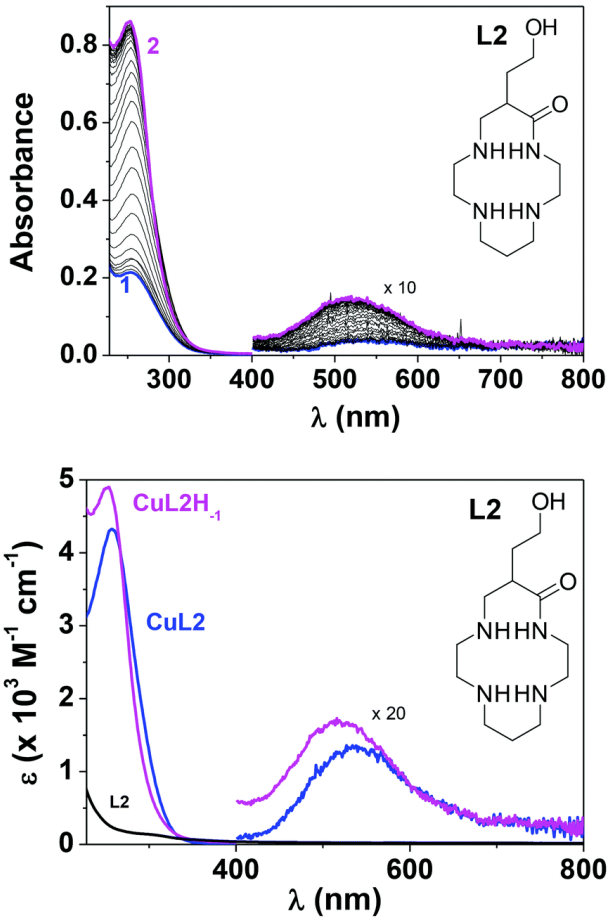

Fig. 4. (Top) UV-vis absorption spectrophotometric *versus* pH titration of the Cu^{2+} complex with ligand **L2**. (Bottom) Electronic absorption spectra of **L2** and its cupric complexes. Solvent: water; I = 0.100(8) M NaCl; T = 25.0(2) °C; $[\mathbf{L2}]_0 = [Cu^{2+}]_0 = 1.87 \times 10^{-4}$ M; (1) pH = 2.31; (2) pH = 6.55. The absorption spectra have not been corrected from dilution effects.

Theoretical calculations. Attempts to obtain single crystals suitable for X-ray diffraction measurements of the cupric complexes with the oxo-cyclam ligands **L2** and **L3** were unfortunately unsuccessful. Thus, the structures of the $[Cu\mathbf{L2}]^{2+}$ and $[Cu\mathbf{L2}\text{-H}]^{+}$ complexes were investigated using density functional theory (DFT) calculations. The X-ray structures of the Cu^{2+}complex with the parent oxo-cyclam ligand show that the ligand adopts a *trans*-III conformation.[29] The ligand provides a square-planar coordination to the Cu^{2+} ion both in its protonated and deprotonated forms, with two additional oxygen donor atoms of water molecules or perchlorate anions providing weak axial coordination (Cu–O distances in the range 2.34–2.84 Å).[30] Thus, we performed geometry optimizations of the $[Cu(\mathbf{L2}\text{-H})(H_2O)_n]^{+}$ and $[Cu(\mathbf{L2})(H_2O)_n]^{2+}$ systems (n = 0–2) at the TPSSh/TZVP level, which showed the calculated structures to be in good agreement with the reference crystallographic data.[31,32] Geometry optimizations of the $[Cu(\mathbf{L2}\text{-H})(H_2O)_2]^{+}$ and $[Cu(\mathbf{L2})(H_2O)_2]^{2+}$ systems resulted in the expulsion of one of the water molecules from the metal coordination environment, while the water molecule in $[Cu(\mathbf{L2}\text{-H})(H_2O)]^{+}$ and $[Cu(\mathbf{L2})(H_2O)]^{2+}$ is shown to have weak apical coordination with the Cu–O distances of 2.46 and 2.41 Å, respectively (Fig. 5). In all optimized structures the ligand adopts a *trans*-III conformation; the complexes of the deprotonated ligand present a rather short Cu–N distance involving the amide nitrogen atom that is lengthened upon protonation of the amide oxygen atom by *ca.* 0.05 Å. The calculated bond distances of the metal coordination environments are in good agreement with those reported for the parent complexes of oxo-cyclam.[30]

Table 5. Electrochemical parameters measured for the Cu^{2+} complexes with **L1–L3** in water at pH 7.4.[a]

	Reduction peak	Oxidation peak
	E_{pc}	E_{pa}
Complex	(V/Ag/AgCl/(3 M KCl))	
$[Cu\mathbf{L1}]^{2+}$	−0.88	—
$[Cu\mathbf{L2}\text{-H}]^{+}$	−0.50	+0.34
$[Cu\mathbf{L3}\text{-H}]^{+}$	−0.87	—

[a] Solvent: H_2O; I = 0.1 M ($NaClO_4$); T = 25.0(2) °C; v = 200 mV s^{-1}.
Reference = Ag/AgCl/3 M KCl. $[Cu\mathbf{L1}]^{2+}$ = $[Cu\mathbf{L2}\text{-H}]^{+}$ = $[Cu\mathbf{L3}\text{-H}]^{+}$ ∼ 1 mM.

The structure of Cu^{2+} complexes of **L2** in solution was further assessed by comparing the experimental d–d absorption bands with the calculated ones for the model systems shown in Fig. 5. This was achieved by using multireference CASSCF/NEVPT2 calculations (see Computational details below), which showed good results for the prediction of d–d transitions of first-row transition metal complexes.[33] Conversely, time-dependent DFT was found to perform poorly.[34] The active space consisted of 9 electrons in the five Cu-based 3d orbitals (CAS(9,5)).

Our calculations performed on $[Cu(\mathbf{L2}\text{-H})]^{+}$ show a simulated absorption spectrum with a maximum at 465 nm, which represents an important deviation from the experimental value (519 nm, Table 4). The absorption profile calculated for $[Cu(\mathbf{L2}\text{-H})(H_2O)]^{+}$ shows a maximum at 495 nm, which is in reasonably good agreement with the experimental value (Fig. 6). The absorption spectrum calculated for the protonated complex $[Cu(\mathbf{L2})(H_2O)]^{2+}$ presents a maximum at the same wavelength, while its intensity is slightly reduced and the absorption profile experiences a slight red shift (Fig. S21, see the ESI[i]). These results are qualitatively in good agreement with the experimental data and therefore confirm that complex protonation occurs at the oxygen atom of the amide group of the ligand. The good agreement between the experimental spectra and those calculated for the $[Cu(\mathbf{L2}\text{-H})(H_2O)]^{+}$ and $[Cu(\mathbf{L2})(H_2O)]^{2+}$ systems suggest that the water

molecule is weakly bound to the metal ion in aqueous solution, providing a square pyramidal coordination environment in agreement with the absence of interactions with chloride anions (*vide supra*, Fig. S13–S17, see the ESI[i]). The broad envelope of the d–d absorption bands calculated for both [Cu(**L2**-H)(H_2O)]$^+$ and [Cu(**L2**)(H_2O)]$^{2+}$ is the result of the contribution of four excitations with comparable oscillator strengths in the range of 460–546 nm for [Cu(**L2**-H)(H_2O)]$^+$ and 472–563 nm for [Cu(**L2**)(H_2O)]$^{2+}$ (Table S1 and Fig. S22, see the ESI[i]).

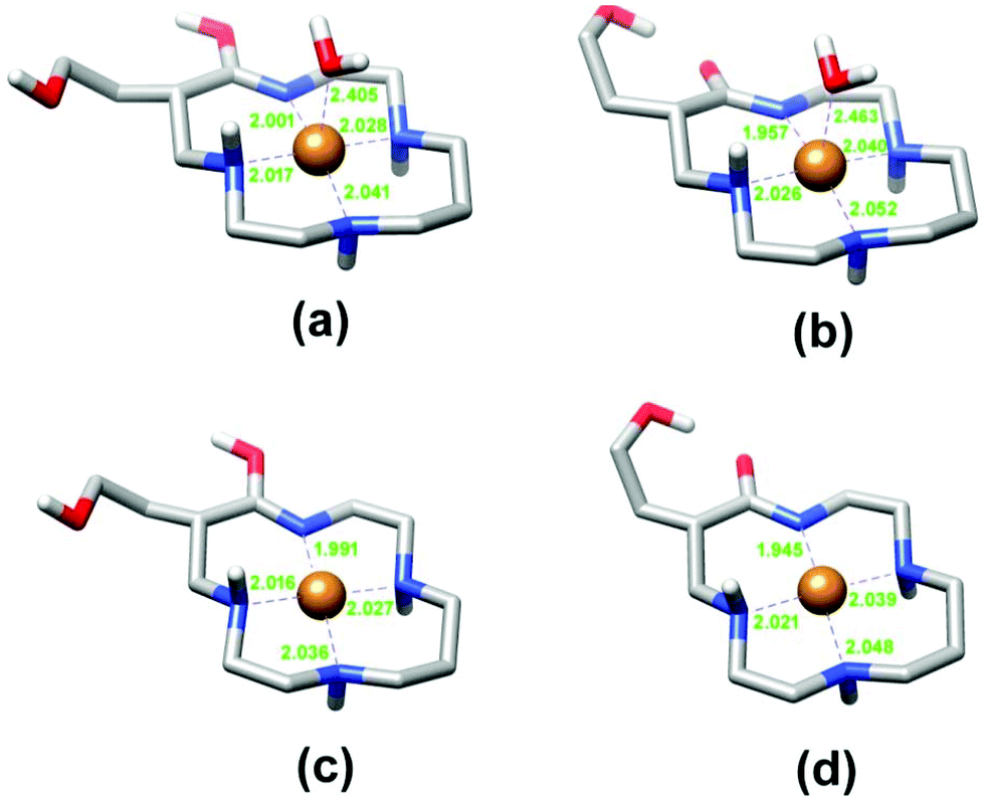

Fig. 5. Structures of (a) [Cu**L2**(H_2O)]$^{2+}$, (b) [Cu**L2**-H(H_2O)]$^+$, (c) [Cu**L2**]$^{2+}$, and (d) [Cu**L2**-H]$^+$ obtained with DFT calculations (TPSSh/TZVP). Bond distances of the metal coordination environments are given in Å.

Conclusions

It is now well recognized that cyclam-based ligands display strong affinities for transition metals and especially for copper(II). These chelators have therefore attracted great interest for several applications requiring a high stability of the complexes, for instance for a safe biological *in vivo* use. However, to achieve this, fine-tuning of the cyclam backbone is still necessary by, for instance, functionalization/alkylation of the endocyclic amine functions. Other subtle chemical modifications can also be performed, such as the replacement of an amine function by an amide one or the introduction of an additional pendant arm *via* one carbon atom of the macrocyclic ring. We have therefore studied the combination of these chemical modifications on the cyclam scaffold on both the acid–base and the copper(II) coordination properties. The previously synthesized cyclam derivative bearing a *C*-appended hydroxyethyl function on a β-*N* position has been either *N*-benzylated (**L1**) and/or substituted by a cyclic amide function that replaces an endocyclic amine group (on the α-*N* position, **L2**/**L3**). Using literature data on various analogues such as cyclam, cyclam-*N*-PrOH and oxo-cyclam, we were able to highlight the major structural effects on the physico-

chemical parameters of the modified cyclam-based chelators. The *N*-benzyl pendant unit has a major influence by decreasing the basicity of the corresponding protonation sites, while the presence of an "oxo"-part lowers the first protonation constant. ESI-MS measurements provided evidence for the exclusive formation of 1 : 1 cupric chelates. Positively monocharged species were systematically characterized. The stability constants measured by pH-metric means then showed that the *C*-appended group has a negligible influence, while *N*-benzylation destabilises the corresponding cupric complexes. By contrast, the "oxo" function significantly increases the stability of the Cu^{2+} complexes. UV-vis absorption *versus* pH measurements demonstrated the comparable involvement of the four nitrogen atoms in **L1**. Furthermore, the high binding constants measured for the copper(II) species with **L2** and **L3** were clearly linked to the deprotonation of the carboxamide unit. Cyclic voltammetry revealed the main presence of the $[Cu\mathbf{L1}]^{2+}$, $[Cu\mathbf{L2}\text{-H}]^{+}$ and $[Cu\mathbf{L3}\text{-H}]^{+}$ species and also the irreversibility of these three systems. Last but not the least, theoretical calculations confirmed that the (de)protonation occurs at the oxygen atom of the amide group for the "oxo" ligands.

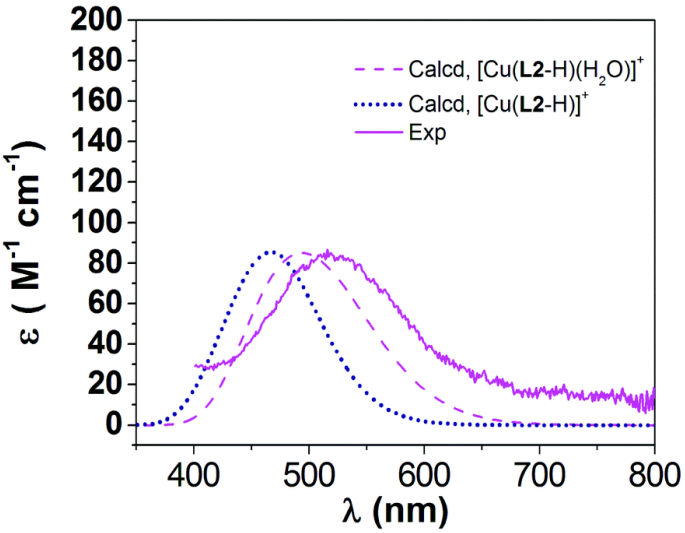

Fig. 6. Visible absorption spectrum of the Cu^{2+} complex of **L2** recorded at pH = 6.55 (solid pink line) and absorption profiles calculated using NEVPT2 calculations based on the CAS(9,5) wave function (dotted blue and dashed pink lines).

C-Functionalized cyclams and especially "oxo"-*C*-functionalized cyclams appear to be very attractive ligands for copper(II) complexation, the additional *C*-appended group presenting no deleterious effect. For biomedical applications (*e.g.* PET imaging), this supplementary function can then be used for bioconjugation with an adequate vector. On the other hand, *N*-alkylation has the detrimental effect of altering the physico-chemical properties of the Cu^{2+} chelates and has to be substituted by a chelating function. The latter must also have the ability to stabilise the chelates independent of their oxidation states, an important outcome in ^{64}Cu-PET imaging.

Experimental section

Starting materials and solvents

Distilled water was purified by passing it through a mixed bed of ion-exchanger (Bioblock Scientific R3-83002, M3-83006) and activated carbon (Bioblock Scientific ORC-83005) and was de-oxygenated by CO_2-

and O_2-free argon (Sigma Oxiclear cartridge) before use. All stock solutions were prepared by weighing solid products on an AG 245 Mettler Toledo analytical balance (precision 0.01 mg). The ionic strength was maintained at 0.100(8) M (ESI^i) with sodium chloride (NaCl, Carlo-Erba-SDS Phar. Eur. 99–100.5%), and all measurements were carried out at 25.0(2) °C. The metal stock solutions (~5–6 × 10^{-2} M) were freshly prepared by the dissolution of appropriate amounts of the corresponding solid perchlorate salts in water saturated with argon. Copper(II) perchlorate ($Cu(ClO_4)_2 \cdot 6H_2O$, Fluka, purum p.a., 99.3%) is a commercial product, which was used without further purification. The metal contents of the solutions were determined according to the classical colorimetric titrations.[35]

Caution! Perchlorate salts combined with organic ligands are potentially explosive and should be handled in small quantities and with adequate precautions.[36]

Potentiometric titrations

The potentiometric titrations of ligands **L1** (1.34 × 10^{-3} M), **L2** (1.36 × 10^{-3} M), and **L3** (1.36 × 10^{-3} M) and their cupric complexes ($1.1 \leq [M]_{tot}/[\mathbf{L}]_{tot} < 1.24$) were performed using an automatic titrator system 794 Basic Titrino (Metrohm) with a combined glass electrode (Metrohm 6.0234.500, Long Life) filled with 0.1 M NaCl in water and connected to a microcomputer (tiamo light 1.2 program for the acquisition of the potentiometric data). The combined glass electrode was calibrated as a hydrogen concentration probe by titrating known amounts of hydrochloric acid (~10^{-1} M from HCl, Sigma-Aldrich, puriss p.a., >37%) with CO_2-free sodium hydroxide solution (~10^{-1} M from NaOH, BDH, AnalaR, 98%).[37] The HCl and NaOH solutions were freshly prepared just before use and titrated with sodium tetraborate decahydrate ($B_4Na_2O_7 \cdot 10H_2O$, Fluka, puriss, p.a., >99.5%) and potassium hydrogen phthalate ($C_8H_5KO_3$, Fluka, puriss, p.a., >99.5%), respectively, using methyl orange (RAL) and phenolphthalein (Prolabo, purum) as the indicators. The cell was thermostated at 25.0 ± 0.2 °C by the flow of a Lauda E200 thermostat. A stream of argon, pre-saturated with water vapor, was passed over the surface of the solution. The Glee program[37] was applied for the glass electrode calibration (standard electrode potential E_0/mV and slope of the electrode/mV pH^{-1}) and to check carbonate levels of the NaOH solutions used (<5%). The potentiometric data of **L1–L3** and their cupric complexes (about 300 points collected over the pH range 2.5–11.5) were refined with the Hyperquad 2000[38] program which uses non-linear least-squares methods.[39] Potentiometric data points were weighted by a formula allowing greater pH errors in the region of an end-point than elsewhere. The weighting factor W_i is defined as the reciprocal of the estimated variance of measurements: $W_i = 1/\sigma_i^2 = 1/[\sigma_E^2 + (\delta E/\delta V)^2 \sigma_V^2]$ where σ_E^2 and σ_V^2 are the estimated variances of the potential and volume readings, respectively. The constants were refined by minimizing the error-square sum, U, of the potentials: at least three potentiometric titrations were treated as single sets, for each system. The quality of fit was judged by the values of the sample standard deviation, S, and the goodness of fit, χ^2, (Pearson's test). At σ_E = 0.1 mV (0.023 σ_{pH}) and σ_V = 0.005 mL, the values of S in different sets of titrations were between 0.6 and 1.2, and χ^2 was below 99. The scatter of residuals *versus* pH was reasonably random, without any significant systematic trends, thus indicating a good fit of the experimental data. The successive protonation constants were calculated from the cumulative constants determined using the program. The uncertainties in the log K values correspond to the added standard deviations in the cumulative constants. The distribution curves of the protonated species of **L1–L3** and their cupric complexes as a function of pH were calculated using the Hyss program.[40]

Spectrophotometric titrations *versus* pH

Spectrophotometric titrations of the cupric complexes with ligands **L1–L3** were thereafter carried out. About 40 mL of solutions containing one equivalent of Cu^{2+} perchlorate and the ligand **Li** (i = 1–3) (for **L1**: $[\mathbf{L1}]_0$ = 1.74 × 10^{-4} M, $[Cu^{2+}]_{tot}$ = 1.75 × 10^{-4} M, 2.37 < pH < 9.48; for **L2**: $[\mathbf{L2}]_0 = [Cu^{2+}]_0$ = 1.87 × 10^{-4} M, 2.31 < pH < 6.55; for **L3**: $[\mathbf{L3}]_0$ = 1.73 × 10^{-4} M, $[Cu^{2+}]_0$ = 1.74 × 10^{-4} M, 2.41 < pH < 7.50; for **L3**: $[\mathbf{L3}]_0 = [Cu^{2+}]_0$ = 1.82 × 10^{-3} M, 2.50 < pH < 5.74) were introduced in a jacketed cell (Metrohm) maintained at

25.0(2) °C (Lauda E200). The free hydrogen ion concentration was measured with a combined glass electrode (Metrohm 6.0234.500, Long Life) and an automatic titrator system 794 Basic Titrino (Metrohm). The Ag/AgCl reference glass electrode was filled with NaCl (0.1 M) (NaCl, Carlo-Erba-SDS Phar. Eur. 99–100.5%) and was calibrated as a hydrogen concentration probe as described above. The initial pH was adjusted to ~2–3 with HCl (Sigma-Aldrich, puriss p.a., >37%), and the titrations of the cupric complexes were then carried out by the addition of known volumes of NaOH solutions (BDH, AnalaR) with an Eppendorf microburette. Special care was taken to ensure that complete equilibration was attained. Absorption spectra*versus* pH were recorded using a Varian CARY 50 spectrophotometer fitted with Hellma optical fibers (Hellma, 041.002-UV) and an immersion probe made of quartz SUPRASIL (Hellma, 661.500-QX). The temperature was maintained at 25.0(2) °C with the help of a Lauda E200 thermostat.

^{1}H NMR *versus* pH titrations

To confirm the pK_a values of **L1** and **L3** ligands, the ^{1}H NMR spectra of 20 mM samples of **L1** and **L3** in D_2O (Merck Uvasol) containing 0.1 M NaCl (Carlo-Erba-SDS Phar. Eur. 99–100.5%) were recorded at 298 K, on a Bruker 500 spectrometer operating at 500 MHz for ^{1}H. 3-(Trimethylsilyl)propionic-2,2,3,3-d_4 acid sodium (TSP, Sigma-Aldrich, 98 atom% D) was used as an internal ^{1}H standard. The combined glass electrode (Metrohm 6.0234.500, Long Life) filled with 0.1 M NaCl in water was calibrated as a hydrogen concentration probe by using a set of commercial Merck buffered solutions (pH 1.68, 4.00, 6.86, 7.41 and 9.18). The pH* values (pH in D_2O solutions measured with the combined glass electrode calibrated with H_2O buffers) of the samples were adjusted using small volumes of concentrated DCl (Sigma-Aldrich, 35 wt% in D_2O, >99 atom % D) or NaOD (Sigma-Aldrich, 40 wt% in D_2O, 99 atom % D). WinEQNMR[41] was used to fit the NMR raw data and provided the pK_a^* values (*i.e.* pK_a measured in D_2O), which compare well with those determined in H_2O by using a pH-metric method. The pK_as reported were obtained by converting the protonation constants measured in D_2O – pK_a^* – into constants valid in H_2O by using the expression $\mathrm{p}K_a = 0.929 \times \mathrm{p}K_a^* + 0.42$.[14]

Analysis and processing of the spectroscopic data

The spectrophotometric data were analyzed with the Specfit[42–44] program which adjusts the absorptivities and the stability constants of the species formed at equilibrium. Specfit uses factor analysis to reduce the absorbance matrix and to extract the eigenvalues prior to the multiwavelength fit of the reduced data set according to the Marquardt algorithm.[45,46]

Electrospray mass spectrometric measurements

Electrospray mass spectra of cupric complexes with **L1–L3** were obtained with an Agilent Technologies 6120 quadrupole equipped with an electrospray (ESI) interface. Solutions (5×10^{-5} M) of the Cu^{2+} complexes with **L^1–L^3** have been prepared in water in the absence of any background salt. The sample solutions were continuously introduced into the spectrometer source with a syringe pump (KD Scientific) with a flow rate of 800 μL h^{-1}. For electrospray ionization, the drying gas was heated at 250 °C and its flow was set at 6 L min^{-1}. The capillary exit voltage was fixed at 5 kV and the skimmer voltage was varied from 100 to 170 V in order to optimize the signal responses. Scanning was performed from *m*/*z* = 100 to 1000 and no fragmentation processes were observed under our experimental conditions.

Electrochemistry

Cyclic voltammetry of the cupric complexes with ligands **L1–L3** (~mM) was performed using a Voltalab 50 potentiostat/galvanostat (Radiometer Analytical MDE15 polarographic stand, PST050 analytical voltammetry and CTV101 speed control unit) controlled by the Voltamaster 4 electrochemical software. A conventional three-electrode cell (10 mL) was employed in our experiments with a glassy carbon disk (GC, s = 0.071 cm^2) set into a Teflon rotating tube as a working electrode, a Pt wire as a counter electrode,

and Ag/AgCl/(3 M KCl) as the reference electrode (+210 mV *vs.* NHE, normal hydrogen electrode).[47] Prior to each measurement, the surface of the GC electrode was carefully polished with a 0.3 μm aluminium oxide suspension (Escil) on a silicon carbide abrasive sheet of grit 800/2400. The GC electrode was then abundantly washed with water and dried with a paper towel and argon. The electrode was installed into the voltammetry cell along with the platinum wire counter electrode and the reference electrode. 10 mL of the buffered aqueous solutions containing *ca*. 10^{-3} M of the cupric complexes with **L1–L3** were vigorously stirred and purged with O_2-free (Sigma Oxiclear cartridge) argon for 15 minutes before the voltammetry experiment was initiated, and it was maintained under an argon atmosphere during the measurement step. The cyclic voltammograms were recorded at room temperature (23(1) °C) in buffered aqueous solution at pH 7.4 (5 mM HEPES, 4-(2-hydroxyethyl)-1-piperazineethanesulfonic acid) and 95 mM $NaClO_4$ as the supporting and inert electrolyte.[48] The voltage sweep rate was varied from 50 to 1000 mV s^{-1} and several cyclic voltammograms were recorded from +1.2 V to −2.0 V. Peak potentials were measured at a scan rate of 200 mV s^{-1} unless otherwise indicated.

Computational details

The geometries of the $[Cu(\mathbf{L2}\text{-H})(H_2O)_n]^+$ and $[Cu(\mathbf{L2})(H_2O)_n]^{2+}$ systems (n = 0–2) were optimized at the TPSSh/TZVP level[49,50] using the Gaussian 09 package (Revision D.01).[51] Bulk solvent effects (water) were included by using the integral equation formalism variant of the polarizable continuum model (IEFPCM),[52] which models the solute cavity as an envelope of spheres with an appropriate radii centred on atoms or atomic groups. The universal force field radii (UFF)[53] scaled by a factor of 1.1 were used to define the solute cavities. No symmetry constraints have been imposed during the optimizations. The stationary points found on the potential energy surfaces as a result of geometry optimizations were checked to represent energy minima rather than saddle points using frequency analysis. The default values for the integration grid (75 radial shells and 302 angular points) and the SCF energy convergence criteria (10^{-8}) were used in all calculations.

Nonrelativistic energy levels and wave functions were computed using the Complete Active Space Self-Consistent Field (CASSCF) method[54] along with the TZVP basis set and the ORCA program package (Version 3.0.3).[55] CASSCF calculations were performed by using an active space including nine electrons distributed into the five Cu 3d-based molecular orbitals (CASS(9,5)). The CASSCF wavefunctions were subsequently analyzed using the N-electron valence perturbation theory to second order (NEVPT2)[56] to account for dynamic correlation. The RIJCOSX approximation[57] was used to speed up both CASSCF and NEVPT2 calculations with the aid of the Def2-TZVPP/JK auxiliary basis set[58] as constructed automatically by ORCA. The spin–orbit contribution was considered employing the spin–orbit mean field approach (SOMF) using the one-center approximation to the exchange term (SOMF(1X)).[42] The convergence tolerances and integration accuracies of the calculations were increased from the defaults using the available TightSCF and Grid7 options (for Cu). Solvent effects (water) were taken into account by using the conductor-like screening model (COSMO)[59] as implemented in ORCA. Absorption spectra were calculated by using the CASSCF/NEVPT2 level including spin–orbit coupling effects by the quasi-degenerate perturbation theory (QDPT).[60] The absorption profiles were simulated using Gaussian functions with a half width at half height of 3000 cm^{-1}.

Conflicts of interest

There are no conflicts of interest to declare.

Acknowledgments

R. T. acknowledges the Ministère de l'Enseignement Supérieur et de la Recherche and the Centre National de la Recherche Scientifique. M. E. thanks the Centre National de la Recherche Scientifique (CNRS). M. E. is also grateful to the New York University Abu Dhabi Undergraduate Research Program for the summer research funding for S. N. C. P.-I. and D. E.-G. acknowledge the Centro de Supercomputación de Galicia (CESGA) for providing the computer facilities.

References

1. (*a*) R. Delgado, V. Félix, L. M. P. Lima and D. W. Price, *Dalton Trans.*, 2007, 2734–2743; (*b*) L. M. P. Lima, D. Esteban-Gómez, R. Delgado, C. Platas-Iglesias and R. Tripier, *Inorg. Chem.*, 2012, **51**, 6916–6927; (*c*) L. M. P. Lima, Z. Halime, R. Marion, N. Camus, R. Delgado, C. Platas-Iglesias and R. Tripier, *Inorg. Chem.*, 2014, **53**, 5269–5279.

2. R. S. Drago, *Inorg. Chem.*, 1973, **12**, 2211–2212.

3. (*a*) P. Scrimin and L. J. Prins, *Chem. Soc. Rev.*, 2011, **40**, 4488–4505; (*b*) F. Bartoli, A. Bencini, L. Conti, C. Giorgi, P. Paoli, P. Rossi, B. Valtancoli, N. Le Bris and R. Tripier, *Org. Biomol. Chem.*, 2016, **14**, 8309–8321.

4. G. Neri, J. J. Walsh, C. Wilson, A. Reynal, J. Y. C. Lim, X. Li, A. J. P. White, N. J. Long, J. R. Durrant and A. J. Cowan, *Phys. Chem. Chem. Phys.*, 2015, **17**, 1562–1566.

5. (*a*) C. R. Munteanu and K. Suntharalingam, *Dalton Trans.*, 2015, **44**, 13796–13808; (*b*) X. Liang and P. J. Sadler,*Chem. Soc. Rev.*, 2004, **33**, 246–266; (*c*) C. J. Anderson and M. J. Welch, *Chem. Rev.*, 1999, **99**, 2219–2234.

6. (*a*) M. D. Bartholomä, *Inorg. Chim. Acta*, 2012, **389**, 36–51; (*b*) S. J. Archibald, *Annu. Rep. Prog. Chem., Sect. A: Inorg. Chem.*, 2009, **105**, 297–322.

7. Y. Sun, D. Chen, A. E. Martell and M. J. Welch, *Inorg. Chim. Acta*, 2001, **324**, 180–187.

8. R. Machida, E. Kimura and M. Kodama, *Inorg. Chem.*, 1983, **22**, 2055–2061.

9. E. Kimura, T. Koike, R. Machida, R. Nagai and M. Kodama, *Inorg. Chem.*, 1984, **23**, 4181–4188.

10. L. C. Siegfried and T. A. Kaden, *J. Phys. Org. Chem.*, 1992, **5**, 549–555.

11. P. Antunes, R. Delgado, M. G. B. Drew, V. Felix and H. Maecke, *Inorg. Chem.*, 2007, **46**, 3144–3153.

12. (*a*) F. Kou, S. Zhu, H. Lin, W. Chen, Y. Chen and M. Lin, *Polyhedron*, 1997, **16**, 2021–2028; (*b*) S. Zhu, F. Kou, H. Lin, M. Lin and Y. Chen, *Inorg. Chem.*, 1996, **35**, 5851–5859; (*c*) T. Benabdallah and R. Guglielmetti, *Bull. Soc. Chim. Fr.*, 1988, **5**, 821–827; (*d*) V. Bernhardt, K. A. Byriel, C. H. L. Kennard and P. C. Sharpe, *Inorg. Chem.*, 1996, **35**, 2045–2052.

13. (*a*) N. Camus, Z. Halime, N. Le Bris, H. Bernard, M. Beyler, C. Platas-Iglesias and R. Tripier, *RSC Adv.*, 2015, **5**, 85898–85910; (*b*) Z. Halime, M. Frindel, N. Camus, P.-Y. Orain, M. Lacombe, M. Chérel, J.-F. Gestin, A. Faivre-Chauvet and R. Tripier, *Org. Biomol. Chem.*, 2015, **13**, 11302–11314; (*c*) N. Camus, Z. Halime, N. Le Bris, H. Bernard, C. Platas-Iglesias and R. Tripier, *J. Org. Chem.*, 2014, **79**, 1885–1899.

14. A. Krężel and W. Bal, *J. Inorg. Biochem.*, 2004, **98**, 161–166.

15. E. Suet and A. Laouenan, *Talanta*, 1986, **33**, 721–727.

16. R. D. Hancock, R. J. Motekaitis, J. Mashishi, I. Cukrowski, J. H. Reibenspies and A. E. Martell, *J. Chem. Soc., Perkin Trans. 2*, 1996, 1925–1929.

17. M. Micheloni, A. Sabatini and P. Paoletti, *J. Chem. Soc., Perkin Trans. 2*, 1978, 828–830.

18. P. J. Davies and K. P. Wainwright, *Inorg. Chim. Acta*, 1999, **294**, 103–108.

19. V. Frenna, N. Vivona, G. Consiglio and D. Spinelli, *J. Chem. Soc., Perkin Trans. 2*, 1985, 1865–1868.

20. R. J. Motekaitis, A. E. Martell and D. A. Nelson, *Inorg. Chem.*, 1984, **23**, 275–283.

21. Y. Moriguchi, M. Hashimoto and K. Sakata, *Fukuoka Kyoiku Daigaku Kiyo, Dai-3-bunsatsu: Sugaku, Rika, Gijutsuka Hen*, 1990, 43.

22. V. J. Thom, G. D. Hosken and R. D. Hancock, *Inorg. Chem.*, 1985, **24**, 3378–3381.

23. R. M. Smith, A. E. Martell and R. J. Motekaitis, *Critical Stability Constants Database 46, version 5*, NIST, Gaithersburg, MD, 1998.

24. W. R. Harris, C. J. Carrano and K. N. Raymond, *J. Am. Chem. Soc.*, 1979, **101**, 2213–2214.

25. R. N. Patel, R. P. Shrivastava, N. Singh, S. Kumar and K. B. Pandeya, *Indian J. Chem.*, 2001, **40A**, 361–367.

26. A. Sornosa Ten, N. Humbert, B. Verdejo, J. M. Llinares, M. Elhabiri, J. Jezierska, C. Soriano, H. Kozlowski, A.-M. Albrecht-Gary and E. Garcia-Espana, *Inorg. Chem.*, 2009, **48**, 8985–8997.

27. N. Wei, N. N. Murthy and D. K. Karlin, *Inorg. Chem.*, 1994, **33**, 6093–6100.

28. D. Grujicic and B. Pesic, *Electrochim. Acta*, 2002, **47**, 2901–2912.

29. X. Liang and P. J. Sadler, *Chem. Soc. Rev.*, 2004, **33**, 246–266.

30. L. Siegfried, M. Neuburger, M. Zehnder and T. A. Kaden, *J. Chem. Soc., Chem. Commun.*, 1994, 951–952.

31. A. Rodríguez-Rodríguez, Z. Halime, L. M. P. Lima, M. Beyler, D. Deniaud, N. Le Poul, R. Delgado, C. Platas-Iglesias, V. Patinec and R. Tripier, *Inorg. Chem.*, 2016, **55**, 619–632.

32. M. Le Fur, M. Beyler, N. Le Poul, L. M. P. Lima, Y. Le Mest, R. Delgado, C. Platas-Iglesias, V. Patinec and R. Tripier, *Dalton Trans.*, 2016, **45**, 7406–7420.

33. S. Ye, C. Kupper, S. Meyer, E. Andris, R. Naveátil, O. Krahe, B. Mondal, M. Atanasov, E. Bill, J. Roithová, F. Meyer and F. Neese, *J. Am. Chem. Soc.*, 2016, **138**, 14312–14325.

34. S. P. de Visser, M. G. Quesne, B. Martin, P. Comba and U. Ryde, *Chem. Commun.*, 2014, **50**, 262–282.

35. *Méthodes d'Analyses Complexométriques avec les Titriplex®*, ed. E. Merck, Darmstadt, 1975.

36. K. N. Raymond, *Chem. Eng. News*, 1983, **61**, 4.

37. P. Gans and B. O'Sullivan, *Talanta*, 2000, **51**, 33–37.

38. (*a*) P. Gans, A. Sabatini and A. Vacca, *HYPERQUAD2000*, Leeds, U.K., and Florence, Italy, 2000; (*b*) P. Gans, A. Sabatini and A. Vacca, *Talanta*, 1996, **43**, 1739–1753.

39. P. Gans, *Data Fitting in the Chemical Sciences*, John Wiley & Sons, Chichester, 1992.

40. L. Alderighi, P. Gans, A. Ienco, D. Peters, A. Sabatini and A. Vacca, *Coord. Chem. Rev.*, 1999, **184**, 311–318.

41. M. J. Hynes, *J. Chem. Soc., Dalton Trans.*, 1993, 311–312.

42. H. Gampp, M. Maeder, C. J. Meyer and A. D. Zuberbühler, *Talanta*, 1985, **32**, 95–101.

43. H. Gampp, M. Maeder, C. J. Meyer and A. D. Zuberbühler, *Talanta*, 1985, **32**, 251–264.

44. H. Gampp, M. Maeder, C. J. Meyer and A. D. Zuberbühler, *Talanta*, 1985, **32**, 1133–1139.

45. D. W. Marquardt, *J. Soc. Ind. Appl. Math.*, 1963, **11**, 431–441.

46. M. Maeder and A. D. Zuberbühler, *Anal. Chem.*, 1990, **62**, 2220–2224.

47. D. T. Sawyer, A. Sobkowiak and J. L. Roberts Jr., *Electrochemistry for Chemists*, 2nd edn, Wiley, New York, 1995, p. 192.

48. K. Izutsu, *Electrochemistry in Nonaqueous Solutions*, Wiley, 2002.

49. J. M. Tao, J. P. Perdew, V. N. Staroverov and G. E. Scuseria, *Phys. Rev. Lett.*, 2003, **91**, 146401.

50. A. Schaefer, C. Huber and R. Ahlrichs, *J. Chem. Phys.*, 1994, **100**, 5829–5835.

51. M. J. Frisch, G. W. Trucks, H. B. Schlegel, G. E. Scuseria, M. A. Robb, J. R. Cheeseman, G. Scalmani, V. Barone, B. Mennucci, G. A. Petersson, H. Nakatsuji, M. Caricato, X. Li, H. P. Hratchian, A. F. Izmaylov, J. Bloino, G. Zheng, J. L. Sonnenberg, M. Hada, M. Ehara, K. Toyota, R. Fukuda, J. Hasegawa, M. Ishida, T. Nakajima, Y. Honda, O. Kitao, H. Nakai, T. Vreven, J. A. Montgomery Jr., J. E. Peralta, F. Ogliaro, M. Bearpark, J. J. Heyd, E. Brothers, K. N. Kudin, V. N. Staroverov, R. Kobayashi, J. Normand, K. Raghavachari, A. Rendell, J. C. Burant, S. S. Iyengar, J. Tomasi, M. Cossi, N. RegaJ. M. Millam, M. Klene, J. E. Knox, J. B. Cross, V. Bakken, C. Adamo, J. Jaramillo, R. Gomperts, R. E. Stratmann, O. Yazyev, A. J. Austin, R. Cammi, C. Pomelli, J. W. Ochterski, R. L. Martin, K. Morokuma, V. G. Zakrzewski, G. A. Voth, P. Salvador, J. J. Dannenberg, S. Dapprich, A. D. Daniels, Ö. Farkas, J. B. Foresman, J. V. Ortiz, J. Cioslowski and D. J. Fox, *Gaussian 09, Revision D.1*, Gaussian, Inc., Wallingford CT, 2009.

52. J. Tomasi, B. Mennucci and R. Cammi, *Chem. Rev.*, 2005, **105**, 2999–3094.

53. A. K. Rappe, C. J. Casewit, K. S. Colwell, W. A. Goddard III and W. M. Skiff, *J. Am. Chem. Soc.*, 1992, **114**, 10024–10035.

54. P.-A. Malmqvist and B. O. Roos, *Chem. Phys. Lett.*, 1989, **155**, 189–194.

55. F. Neese, The ORCA Program System, *Wiley Interdiscip. Rev.: Comput. Mol. Sci.*, 2012, **2**, 73–78.

56. (*a*) C. Angeli, R. Cimiraglia and J.-P. Malrieu, *Chem. Phys. Lett.*, 2001, **350**, 297–305; (*b*) C. Angeli, R. Cimiraglia and J.-P. Malrieu, *J. Chem. Phys.*, 2002, **117**, 9138; (*c*) C. Angeli, R.

Cimiraglia, S. Evangelisti, T. Leininger and J.-P. Malrieu, *J. Chem. Phys.*, 2001, **114**, 10252; (*d*) C. Angeli and R. Cimiraglia, *Theor. Chem. Acc.*, 2002, **107**, 313.

57. (*a*) F. Neese, F. Wennmohs, A. Hansen and U. Becker, *Chem. Phys.*, 2009, **356**, 98–109; (*b*) R. Izsak and F. Neese, *J. Chem. Phys.*, 2011, **135**, 144105; (*c*) T. Petrenko, S. Kossmann and F. Neese, *J. Chem. Phys.*, 2011, **134**, 054116; (*d*) S. Kossmann and F. Neese, *Chem. Phys. Lett.*, 2009, **481**, 240–243.

58. F. Weigend and R. Ahlrichs, *Phys. Chem. Chem. Phys.*, 2005, **7**, 3297–3305.

59. S. Sinnecker, A. Rajendran, A. Klamt, M. Diedenhofen and F. Neese, *J. Phys. Chem. A*, 2006, **110**, 2235–2245.

60. (*a*) D. Ganyushin and F. Neese, *J. Chem. Phys.*, 2006, **125**, 024103; (*b*) F. Neese, *J. Chem. Phys.*, 2005,**122**, 034107.

[i] Electronic supplementary information (ESI) available: Potentiometric titrations of **L1–L3** and their cupric complexes, UV-vis absorption titrations of the cupric complexes with **L1–L3** as a function of pH, ESI-MS spectra, CV of the cupric complexes with **L1–L3**, ^{1}H NMR titrations of **L1** and **L2**, effect of Cl^{-} on the d–d transitions of the metal complexes with **L1–L3**, absorption titration of **L1–L3** by Cu^{2+} at pH 2 and optimized Cartesian coordinates obtained with DFT calculations. See DOI: 10.1039/c7dt00750g.